Chinese Chemical Letters 37 (2026) 111719

Contents lists available at ScienceDirect

Chinese Chemical Letters

journal homepage: www.elsevier.com/locate/cclet

Two-fold gold(I)-catalyzed 7-*endo-dig* annulation toward synthesis of curved azepine-embedded nanographenes

Chenwei Li[a,1], Yijian Ma[a,1], Jun Yu[a,1], Jing Liu[a], Jiang Wang[a], Jiajia Liu[a], Kailiang Ding[a], Manman Sun[b], Chengshuo Shen[a,*], Xunshan Liu[a,*], Maozhong Miao[a,*]

[a] School of Chemistry and Chemical Engineering, Zhejiang Sci-Tech University, Hangzhou 310018, China
[b] Advanced Research Institute and School of Pharmaceutical Science, Taizhou University, Jiaojiang 318000, China

ARTICLE INFO

Article history:
Received 16 May 2025
Revised 26 July 2025
Accepted 12 August 2025
Available online 13 August 2025

Keywords:
Gold catalysis
7-*endo-dig* annulation
Azepine-embedded NGs
Negative curvature
NIR-emission

ABSTRACT

Nanographenes (NGs) incorporating *N*-doped heptagonal units demonstrate intriguing physicochemical properties, attributed to their negatively curved structure induced by the angular strain of the heptagons and the electronic effects of nitrogen atoms, while their precise synthesis remains a challenging task. Herein, we developed an efficient approach for the construction of azepine-embedded NGs *via* two-fold S_NAr/gold(I)-catalyzed 7-*endo-dig* annulation from commercially available 4,7-dibromo-5,6-difluorobenzo[2,1,3]thiadiazole. The fusion of two heptagonal rings dramatically increases the intramolecular strain and forces the central skeleton to twist, giving rise to a unique packing mode in the crystal. The incorporation of thiadiazole leads to a pronounced bathochromic shift in the fluorescence emission, which causes the typical product to display NIR-emission. Furthermore, it is found that the backbone core of these NGs with thiadiazole exhibits excellent single-molecule conductivity as well.

© 2026 Published by Elsevier B.V. on behalf of Chinese Chemical Society and Institute of Materia Medica, Chinese Academy of Medical Sciences.

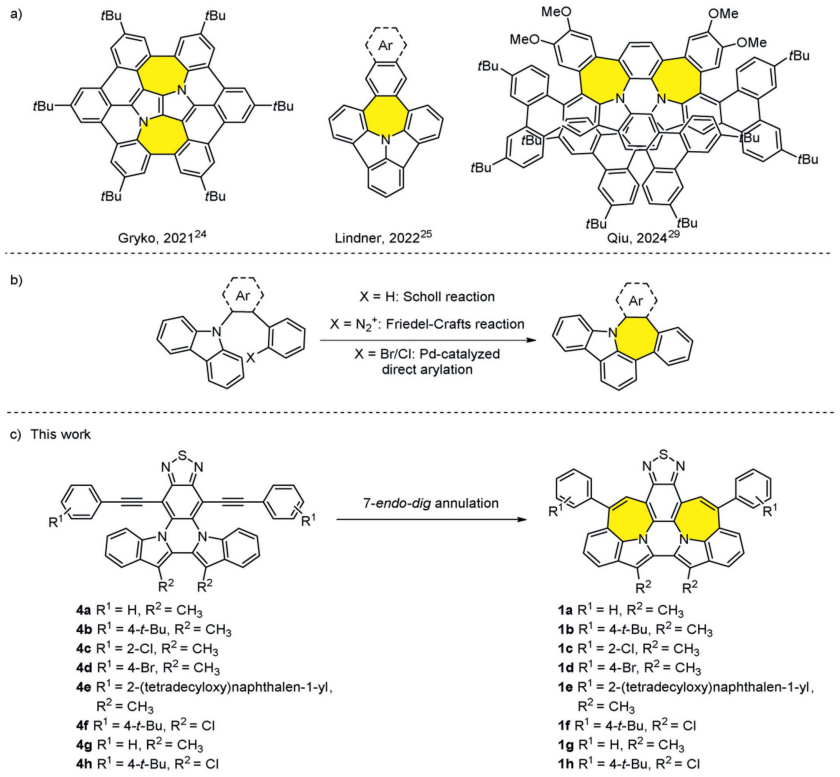
Non-planar nanographenes (NGs) have received widespread attention owing to their unique structures and intriguing properties [1–3], which could be formed by introducing non-planar elements such as helix [4–6], positive curvature [7], or negative curvatures [8–13] to their π-conjugated skeletons. Among them, the negatively curved NGs containing seven- or eight-membered rings display intriguing physicochemical properties including increasing solubility [14], unique antiaromaticity feature [14], additional chirality [15,16], as well as open-shell character [17,18]. Recently, introducing hetero-atoms into the backbone of NGs revealed to be efficiency in increasing the versatility of the structures and properties of NGs [19–22], especially, incorporating nitrogen atoms into the negative curvatures could not only change the electronic structures of NGs but also simplify the synthetic procedures (Scheme 1a) [23–29]. For example, in 2021, a *N*-doped bowl-shaped NG bearing joined pentagons and heptagons that was synthesized *via* multiple arylation steps reported by Gryko *et al.* was recognized as a promising candidate for host-guest supramolecular research [24]. In 2022, Lindner *et al*. synthesized a series of dibenzazepine-embedded NGs *via* direct arylation, exhibiting thermally activated delayed fluorescence properties [25]. Recently, Qiu, Shen *et al*. also reported a series of *N*-doped heptagon-embedded diaza[7]helicene derivatives, revealing unique supramolecular stacking features [29]. For constructing *N*-doped heptagon (or azepine), Scholl reaction, intramolecular Friedel-Crafts reaction, or Pd-catalyzed direct arylation were involved generally (Scheme 1b) [26–29]. Meanwhile, among these limited methods, the reaction substrates were limited owing to the harsh reaction conditions (*e.g.*, high temperature reaction and high toxicity of Pd catalyst) or uncontrollable reaction results (*e.g.*, multiple side reactions and poor regional selectivity) [30]. Therefore, developing more effective methods in a mild conditions and enlarged reaction scope is highly desired.

Currently, homogeneous gold-catalyzed annulation of acetylene derivatives had been represented as a powerful tool for constructing extended π-conjugated systems [31]. We had reported a variety of gold(I)-catalyzed cycloaddition of strained substrates *via* cationic gold interact with π-bonds for preparing heterocycles [32,33]. Herein, a facile approach for the construction of azepine-embedded NGs with saddle-shaped negative curvature *via* gold(I)-catalyzed intramolecular two-fold 7-*endo-dig*-selective annulation was proposed (Scheme 1c).

As shown in Scheme 2a, the Sonogashira coupling of 4,7-dibromo-5,6-difluorobenzo[2,1,3]thiadiazole was firstly taken to afford arylethynyl-benzo[2,1,3]thiadiazole (arylethynyl-BTD) **2**. Then the S_NAr reaction of **2** with bisindole **3** gave arylethynyl-

* Corresponding authors.
E-mail addresses: shenchengshuo@zstu.edu.cn (C. Shen), xliu350@zstu.edu.cn (X. Liu), mmzok@zstu.edu.cn (M. Miao).
[1] These authors contributed equally to this work.

https://doi.org/10.1016/j.cclet.2025.111719
1001-8417/© 2026 Published by Elsevier B.V. on behalf of Chinese Chemical Society and Institute of Materia Medica, Chinese Academy of Medical Sciences.



Scheme 1. (a) Representative examples of negatively curved NGs bearing *N*-heptagonal rings. (b) Various routes for the synthesis of azepine-embedded NGs from carbazole precursors. (c) This work.

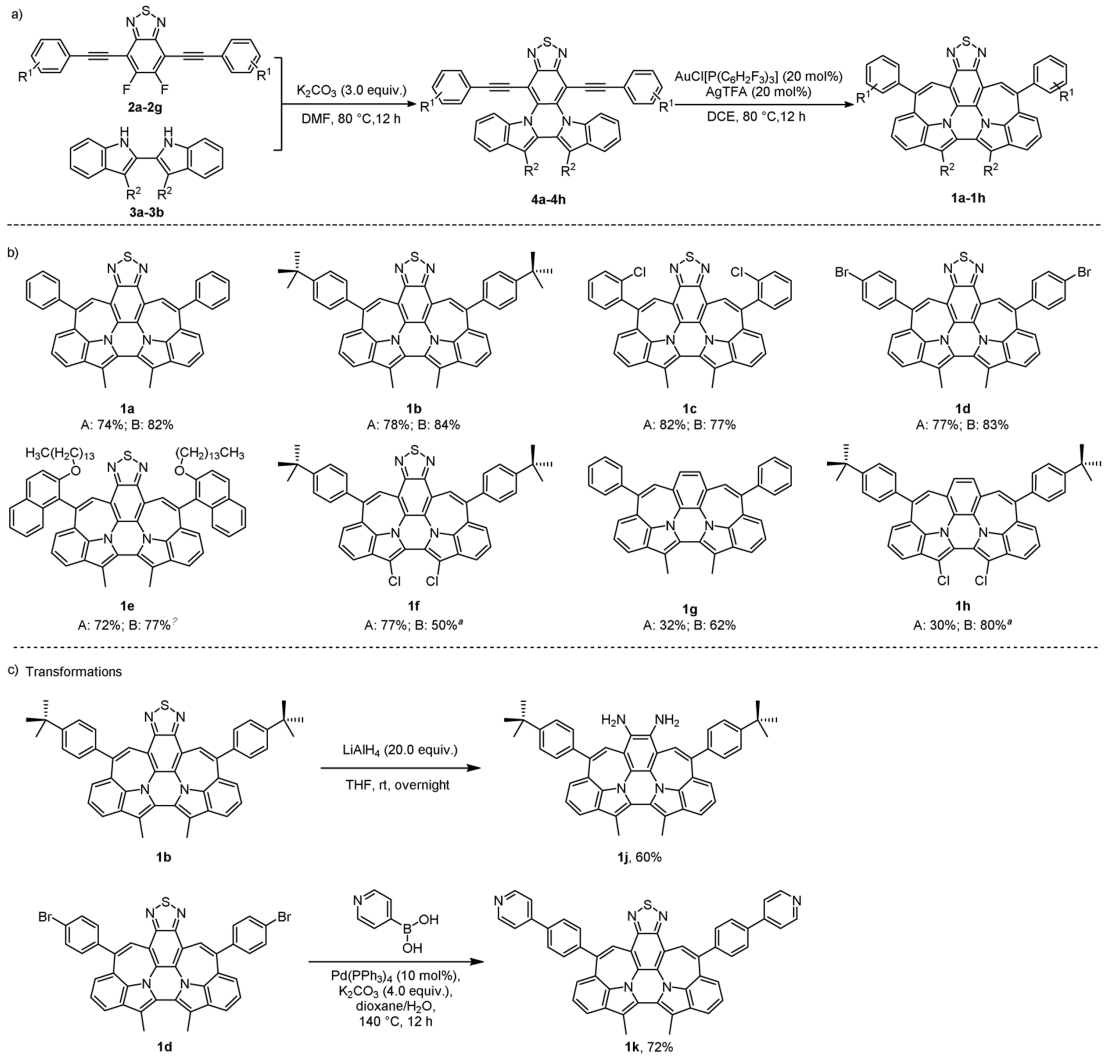
thiadiazoloquinoxaline (arylethynyl-TQ) **4**. Finally, the gold(I)-catalyzed 7-*endo*-*dig* annulation of **4** successfully furnished the targeted NGs **1**. However, the dehydrogenative C-C coupling failed to produce 4,7-dibromo-substituted TQ-framework (Br-TQ) when indole was employed instead of bisindole **3** (path A, Scheme S1 in Supporting information). In addition, only the dehalogenative byproduct was obtained instead of the targeted arylethynyl-TQ **4** when we switched the order of S_NAr reaction and Sonogashira coupling (path B, Scheme S1 in Supporting information).

The reaction conditions of the two-fold S_NAr reaction and gold(I)-catalyzed 7-*endo*-*dig* cyclization processes were optimized, respectively. After checking the solvent, temperature and base effects (Table S1 in Supporting information), the conditions of the S_NAr reaction were established as employing phenylethynyl-BTD **2a** and bisindole **3a** in the presence of 3.0 equiv. K_2CO_3 in DMF at 80 °C for 12 h, producing phenylethynyl TQ **4a** in 74 % isolated yield. Next, the conditions of gold(I)-catalyzed 7-*endo*-*dig* cyclization were evaluated in terms of counterion and ligand effects of gold catalysts (Table S2 in Supporting information), and the suitable conditions were determined as using **4a** catalyzed by 20 mol% of AuCl[$P(C_6H_2F_3)_3$] and AgTFA in DCE at 80 °C for 12 h, affording the corresponding azepine-embedded NG **1a** in 82 % isolated yield.

With optimized conditions in hand, we applied this concept to prepare azepine-embedded NGs with a variety of substitutions (Scheme 2b). Peripheral decorations using different arylacetylenes afforded NGs **1a**-**1e** in high yields in both S_NAr and annulation steps. Bisindole bearing chloro-functionality could be utilized to construct NG **1f**, however, a modest yield (50 %) was obtained in annulation. In addition, the substrates with differential aromaticity were subsequently checked. For example, when the fused-thiadiazole was removed from the substrates, the reaction of both S_NAr and annulation also proceeded smoothly to give donor-NGs **1g** and **1h**, although lower efficiency was observed in S_NAr transformation. It should be noted that the iodocyclization was successfully applied as an alternative to gold(I)-catalyzed 7-*endo*-*dig* annulation to furnish azepine-embedded NG **1i** in 40 % yield (see Supporting information for details). Finally, the transformation of NGs **1** was carried out to showcase the practicality of our method (Scheme 2c). For example, the thiadiazole-functionalized **1b** could be converted to diamino-tethered NG **1j** in 60 % yield, and the pyridyl-group could be introduced based on bromo-containing substrate **1d** *via* Suzuki coupling to afford **1k** in 72 % yield.

Notably, single-crystal X-ray crystallography reveals a saddle-shaped negatively curved structure for **1b**, which exhibits a significantly twisted geometry with C_2 symmetry (Fig. 1a). This intriguing twisted structure leads to a unique packing mode in the crystal. The molecules assemble into dimeric units composed of two enantiomers, displaying anti-parallel, face-to-face stacking with a close intermolecular separation of 3.55 Å. Within this dimer, the distance between the sulfur atom of the thiadiazole ring and the carbon atom bearing a methyl group at the base of the molecular framework is 3.57 Å (Fig. 1b). The close inter-dimer distances suggest the presence of robust π–π stacking interactions. To gain a deeper understanding of the interactions within the dimer, we performed electrostatic potential (ESP) analysis [34] and the independent gradient model based on Hirshfeld partition (IGMH) [35] using Gaussian 09 [36] and Multiwfn 3.8-dev program [37,38]. The ESP analysis reveals a pronounced electronegative region near the nitrogen atom of the thiadiazole ring and an electropositive region adjacent to the methyl group (Fig. 1c), which rationalizes the observed face-to-face packing mode. Furthermore, the IGMH maps for both the entire molecular framework and the interactions between the thiadiazole and methyl groups further corroborate this conclusion (Fig. 1d).

The benzo[2,1,3]thiadiazole (BTD) unit had a large influence on the electronic structures of the nanographenes. The π-electrons



Scheme 2. (a) Selected routes for entering azepine-embedded NGs **1**. (b) Yields of azepine-embedded NGs **1**. A: Yield of the two-fold S_NAr reaction, B: Yield of the two-fold gold(I)-catalyzed 7-*endo-dig* cyclization. [a] Replace AuCl[P($C_6H_2F_3$)$_3$] with AuCl[P(C_6F_5)$_3$]. DCE: 1,2-dichloroethane. (c) Transformations of azepine-embedded NGs **1**.

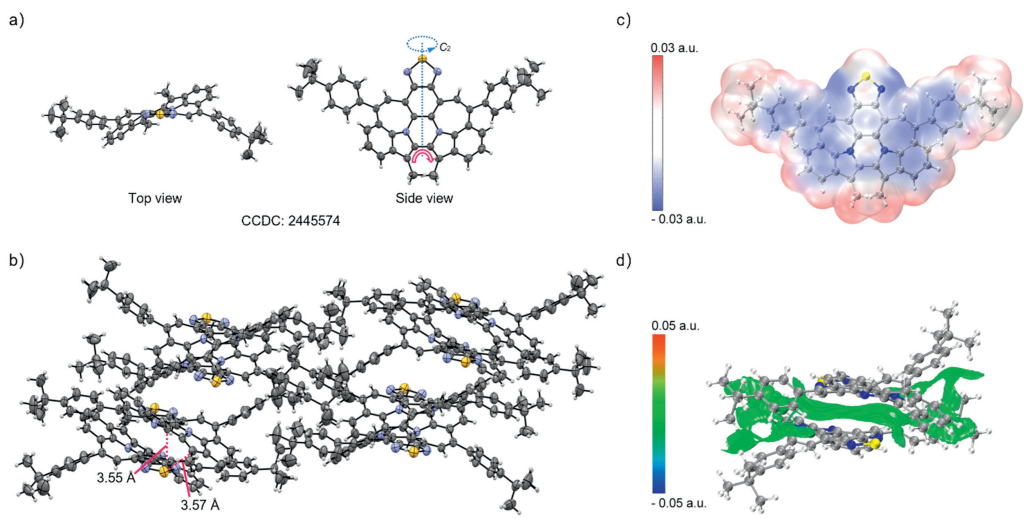


Fig. 1. (a) X-ray crystal structure of **1b**. (b) Packing mode of **1b**. (c) Electrostatic potential (ESP) colored molecular van der Waals surface map of **1b**. (d) Independent gradient model based on Hirshfeld partition (IGMH) map for the dimer (isovalue: 0.0008).

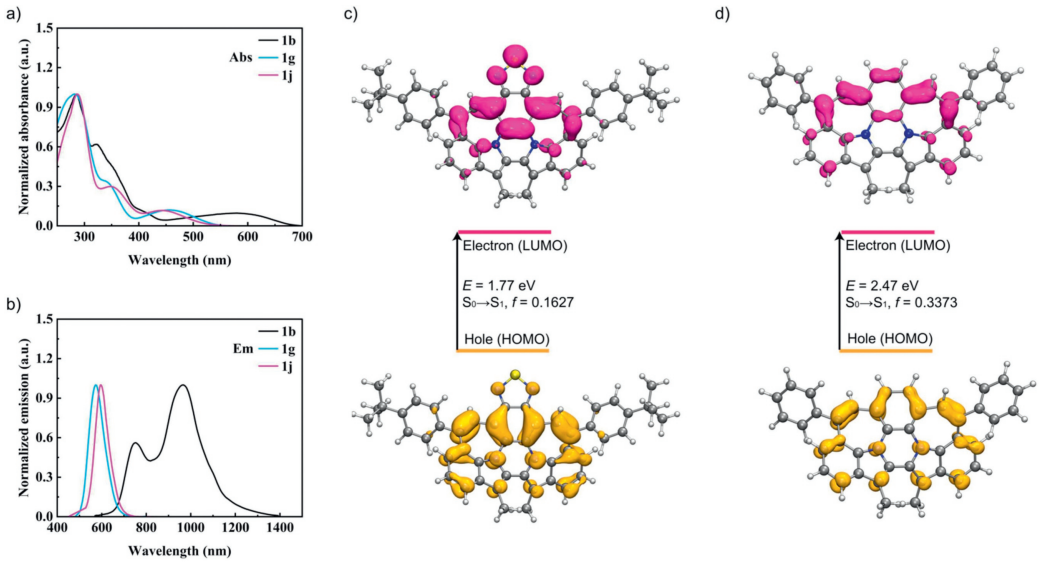


Fig. 2. (a) UV-vis-absorption spectra of **1b**, **1g** and **1j**. (b) Emission spectra of **1b**, **1g** and **1j**. (c) Hole-electron analysis for $S_0 \rightarrow S_1$ transition of **1b** (isovalue: 0.002). (d) Hole-electron analysis for $S_0 \rightarrow S_1$ transition of **1g** (isovalue: 0.002).

largely changed on the adjacent benzene rings when the BTD unit was added (Figs. S17 and S18 in Supporting information). As a result, the emission of **1b** bearing BTD moiety showed a dramatic bathochromic shift (753 nm, 967 nm) compared to **1g** (573 nm) and **1j** (597 nm) for the lower-energy band in DCM (10^{-5} mol/L) (Fig. 2a), and the solid-state fluorescence emission of **1b** (787 nm, 962 nm) and **1g** (615 nm) also proves a dramatic bathochromic shift (Fig. S4 in Supporting information). The frontier molecular orbitals and energy levels of **1b** based on optimized structures elucidated their electronic characteristics (Fig. S10 in Supporting information). The results reveal that the highest occupied molecular orbital (HOMO) of **1b** is delocalized throughout the main part of the molecular framework, whereas the lowest unoccupied molecular orbital (LUMO) is predominantly localized on the BTD ring, the adjacent benzene ring, as well as the two seven-membered rings. The transition analysis showed that the $S_0 \rightarrow S_1$ transition is primarily driven by the HOMO and LUMO, contributing 98.4 % to the excitation, and the calculated excitation energy revealed to be 1.77 eV. The hole-electron analysis also showed a similar conclusion that the excitation nature of $S_0 \rightarrow S_1$ could be interpreted as a partial charge transfer process (Fig. 2c) [39]. On the contrary, **1g** with the absence of the BTD rings displayed a considerable blue shift in their absorption spectra compared with **1b**. For **1g**, the $S_0 \rightarrow S_1$ transition is identified as the local excitation with the electronic delocalization majorly on the main part of the molecular framework for both HOMO and LUMO (Fig. 2d). The excitation energy for $S_0 \rightarrow S_1$ revealed to be 2.47 eV, which is much larger compared to **1b**. In the case of **1j**, the lower-energy band could be contributed to two degenerated excitations of HOMO $\rightarrow$ LUMO and HOMO$-1 \rightarrow$ LUMO, and the excitation energies were even larger than **1b**, which were calculated as 2.50 and 2.57 eV, respectively (Fig. S14 in Supporting information). For the emission spectra of **1b**, **1g** and **1j**, similarly, **1b** showed much more red-shifted for the emission maximum compared to **1g** and **1j** (967 nm *vs.* 573 and 597 nm), where the emission of **1b** was majorly at near infrared region while for **1g** and **1j** the emission showed an orange color. This significant difference in emission spectra might also be attributed to the electronic structures of the molecular π-system that were strongly influenced by the BTD unit. Compared to normal azepine-embedded NGs without thiadiazole ring [23–29], **1b** has a larger emission wavelength and showed NIR emission. In addition, the fluorescence emission of **1b** is close to that of reported nanoparticles (NPs) bearing thiadiazoloquinoxaline centers to a certain extent [40–43], thus, it holds promise in the field of biomedical imaging.

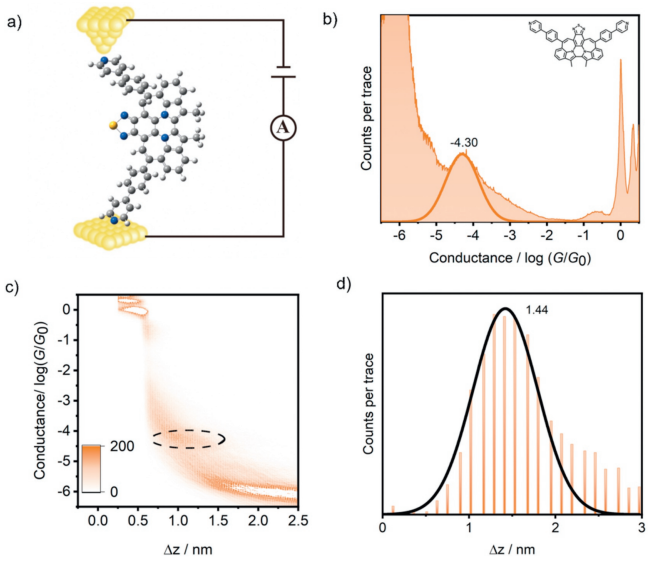


Fig. 3. (a) Schematic diagram of conductivity experiment principle for **1k**. (b) The 1D conductance histograms for **1k**. (c) The 2D conductance histogram for **1k**. d) The plateau length statistics for **1k**.

A pivotal challenge in semiconductor molecular engineering lies in precisely tailoring the intramolecular charge transport properties of π-conjugated frameworks, which serve as fundamental building blocks for semiconductor materials. While single-molecule electronics provide critical techniques for precise characterization of charge transport in tailored systems. Due to the narrow energy gap of molecule **1b**, which enhances its potential as a novel building block of semiconducting materials, we further functionalized it with two pyridine terminating groups, forming a molecular wire **1k** featuring a π-delocalized backbone. We then investigated its single-molecule conductivity using the scanning tunneling microscopy break-junction (STM-BJ) [44–46] technique (Fig. 3a). First, we conducted control experiments in pure 1,2,4-trichlorobenzene (TCB) solvent confirmed the absence of solvent-derived conduc-

tance signals ($G < 10^{-6}$ G_0 at 0.1 V) (Fig. S5 in Supporting information), ensuring subsequent measurements in 0.1 mmol/L **1k** solution exclusively captured single-molecule junctions. Statistical analysis of 2,000 conductance traces revealed a well-defined peak at $10^{-4.30\pm0.02}$ G_0 (Fig. 3b), demonstrating superior charge transport efficiency attributed to the engineered π-system. Furthermore, the measured plateau length (1.44 nm) (Figs. 3c and d), combined with Au electrode snap-back correction (0.5 nm) [47], yielded a molecular junction length of 1.94 nm, aligning remarkably with **1k** length 2.0 nm (Fig. S6 in Supporting information), thereby validating both the structural integrity of the junctions and the experimental precision.

In summary, an efficient synthesis of curved azepine-embedded NGs *via* a step-wise S_NAr/gold(I)-catalyzed 7-*endo*-*dig* annulation was established. The resulting compound **1b** displays NIR-emission ($\lambda_{max,em} = 967$ nm). The computed results reveal that the electronic structure differences lead to a significantly lower $S_0 \rightarrow S_1$ excitation energy for **1b** compared to **1g** and **1j**, inducing a pronounced red shift in the spectrum of **1b** compared to **1g** and **1j**. The conductivity results of **1k** establish its backbone core **1b** as a promising semiconductor building block, meeting organic material performance thresholds. By directly linking π-conjugation optimization to excellent charge transport properties, this work not only advances molecular electronics but also provides a blueprint for the rational development of functional materials. These azepine-embedded NGs may showcase high potential in the area of optoelectronic materials.

Declaration of competing interest

We declare that we have no financial and personal relationships with other people or organizations that can inappropriately influence our work, there is no professional or other personal interest of any nature or kind in any product, service and/or company that could be construed as influencing the position presented in, or the review of, the manuscript entitled.

CRediT authorship contribution statement

Chenwei Li: Writing – original draft, Methodology, Investigation. **Yijian Ma:** Software, Methodology, Investigation. **Jun Yu:** Methodology, Investigation. **Jing Liu:** Investigation, Formal analysis. **Jiang Wang:** Validation, Investigation. **Jiajia Liu:** Validation, Investigation. **Kailiang Ding:** Validation, Investigation. **Manman Sun:** Resources, Formal analysis. **Chengshuo Shen:** Writing – review & editing, Supervision, Project administration. **Xunshan Liu:** Writing – review & editing, Supervision, Resources, Methodology. **Maozhong Miao:** Writing – review & editing, Supervision, Project administration, Investigation, Funding acquisition.

Acknowledgments

The authors are grateful to the Natural Science Foundation of Zhejiang Province (Nos. LY24B020003, LY23B040003), and the Science Foundation of Zhejiang Sci-Tech University (Nos. 22062026-Y and 25262156-Y) for financial support.

Supplementary materials

Supplementary material associated with this article can be found, in the online version, at doi:10.1016/j.cclet.2025.111719.

References

[1] Z.S. Wu, Y.Z. Tan, S. Zheng, et al., J. Am. Chem. Soc. 139 (2017) 4506–4512.
[2] M. Takeda, S. Hiroto, H. Yokoi, et al., J. Am. Chem. Soc. 140 (2018) 6336–6342.
[3] H.A. Lin, Y. Sato, Y. Segawa, et al., Angew. Chem. Int. Ed. 57 (2018) 2874–2878.
[4] Y. Wang, Z.G. Wu, F. Shi, Chem. Cat. 2 (2022) 3077–3111.
[5] H. Shi, B. Xiong, Y. Chen, et al., Chin. Chem. Lett. 34 (2023) 107520.
[6] W. Cui, Z. Jin, W. Fu, C. Shen, Chin. Chem. Lett. 35 (2024) 109667.
[7] E.M. Muzammil, D. Halilovic, M.C. Stuparu, Commun. Chem. 2 (2019) 58.
[8] S.H. Pun, Q. Miao, Acc. Chem. Res. 51 (2018) 1630–1642.
[9] I.R. Márquez, S. Castro-Fernández, A. Millán, et al., Chem. Commun. 54 (2018) 6705–6718.
[10] I.A.Stepek Chaolumen, K.E. Yamada, et al., Angew. Chem. Int. Ed. 60 (2021) 23508–23532.
[11] G. González Miera, S. Matsubara, H. Kono, et al., Chem. Sci. 13 (2022) 1848–1868.
[12] S.H. Pun, Y. Wang, M. Chu, et al., J. Am. Chem. Soc. 141 (2019) 9680–9686.
[13] K.Y. Cheung, Q. Miao, Chin. Chem. Lett. 30 (2019) 1506–1508.
[14] B. Liu, M. Chen, X. Liu, et al., J. Am. Chem. Soc. 145 (2023) 28137–28145.
[15] M. Rickhaus, M. Mayor, M. Jurícek, Soc. Rev. 46 (2017) 1643–1660.
[16] K. Kato, K. Takaba, S. Maki-Yonekura, et al., J. Am. Chem. Soc. 143 (2021) 5465–5469.
[17] J. Liu, S. Mishra, C.A. Pignedoli, et al., J. Am. Chem. Soc. 141 (2019) 12011–12020.
[18] M.W. Wang, Z. Li, Y. Liu, et al., Org. Chem. Front. 10 (2023) 2808–2812.
[19] J. Liu, X. Feng, Synlett 31 (2020) 211–222.
[20] A. Borissov, Y.K. Maurya, L. Moshniaha, et al., Chem. Rev. 122 (2022) 565–788.
[21] K. Bartkowski, P.Z. Crocomo, M.A. Kochman, et al., Chem. Sci. 13 (2022) 10119–10128.
[22] X. Tian, K. Shoyama, F. Würthner, Chem. Sci. 14 (2023) 284–290.
[23] L. Ruan, W. Luo, H. Zhang, et al., Chem. Sci. 15 (2024) 1511.
[24] M. Krezeszewski, Ł. Dobrzycki, A.L. Sobolewski, et al., Angew. Chem. Int. Ed. 60 (2021) 1499815005.
[25] J. Wagner, P.Z. Crocomo, M.A. Kochman, et al., Angew. Chem. Int. Ed. 61 (2022) e202202232.
[26] D. Hellwinkel, H. Seifert, Chem. Ber. 105 (1972) 880–906.
[27] C. Wang, Z. Deng, D.L. Phillips, J. Liu, Angew. Chem. Int. Ed. 62 (2023) e202306890.
[28] S. Qiu, A.C. Valdivia, W. Zhuang, et al., J. Am. Chem. Soc. 146 (2024) 16161–16172.
[29] F. Gan, G. Zhang, J. Liang, C. Shen, H. Qiu, Angew. Chem. Int. Ed. 63 (2024) e202320076.
[30] H. Luo, J. Liu, Angew. Chem. Int. Ed. 63 (2024) e202410759.
[31] C.M. Hendrich, K. Sekine, T. Koshikawa, et al., Chem. Rev. 121 (2021) 9113–9163.
[32] S. Zhang, A. Tang, P. Chen, et al., Org. Lett. 22 (2020) 848–853.
[33] S. Zhang, R. Xie, A. Tang, et al., Org. Lett. 22 (2020) 3056–3061.
[34] J. Zhang, T. Lu, Chem. Chem. Phys. 23 (2021) 20323–20328.
[35] T. Lu, Q. Chen, J. Comput. Chem. 43 (2022) 539–555.
[36] M.J. Frisch, G.W. Trucks, H.B. Schlegel, et al., Gaussian 09, 2013 Revision E.01, Wallingford CT.
[37] T. Lu, F. Chen, Chem. J. Comput. Chem. 33 (2012) 580–592.
[38] T. Lu, J. Chem. Phys. 161 (2024) 082503.
[39] Z. Liu, T. Lu, Q. Chen, Carbon 165 (2020) 461–467.
[40] S. Li, C. Yin, R. Wang, et al., ACS Appl. Mater. Interfaces 12 (2020) 20281–20286.
[41] J. Cui, F. Zhang, D. Yan, et al., Adv. Mater. 35 (2023) 2302639.
[42] M. Liang, L. Liu, Y. Sun, et al., Aggregate 5 (2024) e458.
[43] B. Li, W. Wang, L. Zhao, et al., Adv. Mater. 36 (2024) 2305378.
[44] W. Chen, H. Li, J.R. Widawsky, et al., J. Am. Chem. Soc. 136 (2014) 918–920.
[45] L. Chen, Z. Yang, Q. Lin, et al., Langmuir 40 (2024) 1988–2004.
[46] B. Wang, C. Chen, Y. Huo, et al., J. Am. Chem. Soc. 147 (2025) 7809–7816.
[47] A. Feng, Y. Zhou, M.A.Y. Al-Shebami, et al., Nat. Chem. 14 (2022) 1158–1164.